Laser Chem. 1988, Vol. 8, pp. 283–302

Kinematic Effects on Laser-induced Fluorescence Measurements Performed in Reactive Crossed Beam Experiments

CHRISTIAN NAULIN, MICHEL COSTES, ASMAE BENSEDDIK AND GÉRARD DORTHE

Laboratoire de Photophysique Photochimie Moléculaire†, UA 348, Université de Bordeaux 1, 33405 Talence Cedex, France

(Received November 25, 1987; in final form February 2, 1988)

A simple, realistic model is developed to take into account kinematic effects on laser-induced fluorescence (LIF) measurements in crossed beam reactive scattering experiments. The conversion factor from nascent populations to measured densities (which are proportional to the LIF intensity) is calculated for several cases of practical interest. The density-flux transformation proposed by Zare and coworkers arises from the model as a limiting case. Results concerning the C + NO → CN + O reaction, studied in a pulsed crossed supersonic beam experiment, are also included. Calculations carried out under various conditions emphasize the dramatic importance of beam collimation and pulse duration on detection efficiency.

KEY WORDS: Laser-induced fluorescence, reactive scattering, crossed molecular beams.

I. INTRODUCTION

An unmatched advantage of reactive collision experiments performed with crossed molecular beams is that nascent products are analyzed, with their initial internal quantum states and also the magnitude and direction of their recoil velocity vector. The last feature can, however,

† And GRECO 87 (CNRS) "Dynamique des Réactions Moléculaires."

become puzzling when the laser-induced fluorescence technique is performed at the crossing point, in order to perform internal energy state analysis and deduce state-to-state cross-sections and rate constants.[1] Products in different internal energy states expand in space at different laboratory velocities, $\mathbf{v}_{lab}$, and the densities, which are measured by LIF, do not actually correspond to product fluxes. Clearly, products recoiling at low laboratory velocities are detected more efficiently than those recoiling at high laboratory velocities.

The problem is not acute for reactions releasing little energy because all products recoil with $\mathbf{v}_{lab}$ vectors not very different from the center of mass velocity vector, $\mathbf{v}_{cm}$. A similar situation imposed by the conservation of linear momentum occurs for very exoergic reactions of the type H + H'L (heavy + heavy–light) $\rightarrow$ HH' + L.[1,2] In other situations angular distributions should be considered.

Up to now the only manner to tackle the problem was to perform the density-flux (DF) transformation introduced by Zare and coworkers[2] in the early LIF crossed-beam experiments. However, systematic use of this DF transformation is not always correct. A steady state has to be reached and this requirement is not necessarily fulfilled, especially with pulsed molecular beams of narrow temporal width. Moreover, the laser beam section, relative to the reaction zone, can be of great importance if molecules produced outside the irradiated volume and scattered into it also contribute to the signal. The latter holds in most experiments and in that case product densities in the irradiated volume are dependent on the outcome of reactive collisions happening outside. In this paper we develop a simple realistic model to evaluate the conversion function from nascent populations to measured densities (NPMD) defined by the spatial and temporal overlap of the molecular beams. This model is applied to our experiments dealing with the pulsed crossed supersonic molecular beam study of C + NO $\rightarrow$ CN + O reaction.

Before developing the model, it is worth noting that the present paper does not deal with basic LIF processes, such as polarization or saturation effects, since they have been already studied quite extensively.[3–6] In particular, the problem of multipole orientation may be of crucial importance in LIF measurements: it has been well documented by Greene and Zare,[4] who have specialised the LIF theory for the most commonly occurring experimental geometry, i.e. axially symmetric systems. Saturation of the absorption transition can

also significantly alter the appearance of the spectrum: such effects have been reviewed by Altkorn and Zare,[5] whereas a both theoretical and experimental study of coherent saturation has been recently published by Billy *et al.*[6] In our calculations, all these effects, together with experimental factors, are condensed into a single parameter, B (see below, Eq. 3). When product alignment is negligible, polarization need not be taken into account, and the B parameter can be regarded as constant with respect to orientation effects. In other cases, B may also depend upon product recoil angle. However, this dependence must be considered only in the final step of calculation, namely when integrating over recoil velocity distribution, and therefore has no influence on the main steps of the calculations developed hereafter.

II. THE MODEL

The basic principle of the model is that LIF detection is subject to the constraint that any molecule, produced at time t, anywhere in the space, in a given internal state, and recoiling with a given velocity, will contribute to the signal if, and only if it is present in the detection zone at the probing time. Such a problem cannot be simply solved in the general case, but may be greatly simplified if some assumptions, consistent with cases of practical interest, are made concerning the beam sources and LIF detection.

The model is primarily intended to apply to pulsed beam experiments, but may be easily extended to continuous beams (see below). In both cases, the molecular beams are considered as "ideal." i.e. divergence and velocity spread are neglected. This assumption is quite reasonable for collimated supersonic sources, but can be no longer valid for uncollimated sources, especially if the reaction zone lies in the vicinity of one of the nozzles. Detection is considered to be achieved at a time scale sufficiently short, compared to species time of flight through the detection zone, to ensure that LIF signal processing remain independent of product recoil velocities. The latter condition is generally fulfilled when a pulsed laser, combined with a boxcar integrator, is used for LIF measurement, resulting in a detection time typically much shorter than 1 μs (including laser pulsewidth, and integrator gate aperture delay and duration). Indeed, the present model cannot be applied when a cw laser is used. In that case, the

number of system degrees of freedom cannot be reduced, and a more general method must be used.[7]

II.1. Principles

Consider a three atom reaction, $A + BC \rightarrow AB + C$. Let $[A]$ and $[BC]$ be the number densities of A atoms and BC molecules, respectively. The production rate per unit volume of AB molecules in a particular (v,J) internal state with a given velocity vector in the laboratory frame is expressed as:

$$d[AB(v,J,\mathbf{v}_{\text{lab}})]/dt = \sigma(v,J,\mathbf{v}_{\text{lab}})v_r\,[A][BC] \tag{1}$$

where:

$$\sigma(v,J,\mathbf{v}_{\text{lab}}) = \sigma_R P(v,J) dP^{v,J}(\mathbf{v}_{\text{lab}})/\mathrm{d}\mathbf{v}_{\text{lab}} \tag{2}$$

is a differential reactive cross-section, v_r the reactant relative velocity, σ_R the total reactive cross-section, $P(v,J)$ the product rovibrational distributions, and $dP^{v,J}(\mathbf{v}_{\text{lab}})$ the fraction of molecules $AB(v,J)$ produced with a velocity vector lying between $\mathbf{v}_{\text{lab}}$ and $\mathbf{v}_{\text{lab}} + \mathrm{d}\mathbf{v}_{\text{lab}}$. The dependences of all these factors upon v_r and reactant internal energy states have been dropped for simplicity.

The LIF signal intensity of the corresponding line is proportional to the number of AB molecules in the (v,J) state, $N\{AB(v,J)\}$, present in the probed volume, ΔV_0, at the probing time, considered hereafter as the origin of time, and taken at the end of probe laser pulse:

$$I(v,J) = BN\{AB(v,J)\} \tag{3}$$

where B includes all factors defined in the Breit formula,[1] such as detection quantum yield, together with absorption and emission transition probabilities. In case of saturation, absorption line strengths need not be considered, if the strengths of all the transitions composing the spectrum are approximately the same.[5]

Signal intensity can thus be obtained by integration over time and space of the production rate (Eq. 1) with the condition, referred to as detection constraint in the following, that any molecule, produced in the $d\tau$ volume element at the point $M(x,y,z,t)$ with velocity $\mathbf{v}_{\text{lab}}$, will

contribute to the signal if it is present at the crossing point, O, at the probing time, $t = 0$:

$$I(v,J) = B \int_{(\mathbf{v}_{lab}\, t=OM)} dt \int d\tau \int d\mathbf{v}_{lab} d[AB(v,J,\mathbf{v}_{lab})]/dt \tag{4}$$

II.2. Kinematics

At this point, we must define the collision kinematics for a crossed beam experiment. For simplicity, the two beams will be assumed to cross at right angles, as it is the most frequent configuration. The kinematics are shown in Figure 1. Symbols and notations used hereafter are defined in Table I.

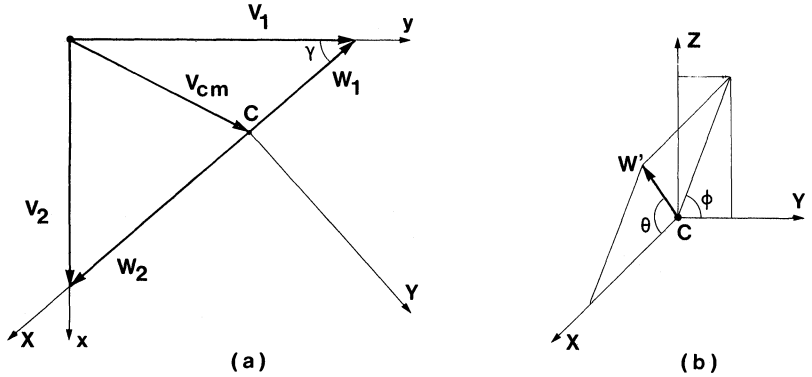

Figure 1 Schematic of the collision kinematics; a: reactants; b: probed product in the cm frame.

The projection of the product recoil velocity vector, $\mathbf{v}_{lab}$, in the laboratory frame is:

$$\begin{aligned} v_x &= w_1 \sin\gamma + w'_X \sin\gamma + w'_Y \cos\gamma \\ v_y &= w_2 \cos\gamma - w'_X \cos\gamma + w'_Y \sin\gamma \\ v_z &= w'_Z \end{aligned} \tag{5}$$

where the w'_j stand for the velocity components in the center of mass (cm) frame, and $\sin\gamma = v_2/v_r$.

Table I Kinematics notations and symbols.

	Reactants		
	Molecule (BC)	Atom (A)	Notes
mass	m_1	m_2	$M = m_1 + m_2$
reduced mass	η		$\mu = m_1 m_2 / M$
velocity			
–lab. frame	$\mathbf{v}_1$	$\mathbf{v}_2$	$v_r^2 = v_1^2 + v_2^2$
–cm frame	$\mathbf{w}_1$	$\mathbf{w}_2$	$v_r = w_1 + w_2$
	$w_1 = \lambda_1 v_r$	$w_2 = \lambda_2 v_r$	$\lambda_i = \eta / m_i$

	Products	
Molecule (AB)	Atom (C)	Notes
$m_1' = m'$	m_2'	$M = m' + m_2'$
η'		$\mu' = m' m_2' / M$
$\mathbf{v}_1' = \mathbf{v}_{\text{lab}}$	$\mathbf{v}_2'$	$\mathbf{v}_{\text{lab}} = \mathbf{v}_{\text{cm}} + \mathbf{w}'$
$\mathbf{w}_1' = \mathbf{w}'$	$\mathbf{w}_2'$	$v_r' = w' + w_2'$
$w_X' = w' \cos\theta$		
$w_Y' = w' \sin\theta \cos\phi$		
$w_Z' = w' \sin\theta \sin\phi$		

Conservation of linear momentum gives:

$$w' = (2\mu' \epsilon_{\text{trans}}')^{1/2} / m' \tag{6}$$

where $\epsilon_{\text{trans}}' = \frac{1}{2} \mu' v_r'^2$ is the product translational energy in the cm frame. Energy balance can be expressed as:

$$\epsilon_{\text{trans}} - \Delta\epsilon_0 + \epsilon_{\text{int}}(A) + \epsilon_{\text{int}}(BC) = \epsilon_{\text{trans}}' + \epsilon_{\text{int}}'(AB) + \epsilon_{\text{int}}'(C) \tag{7}$$

where $\epsilon_{\text{trans}} = \frac{1}{2} \mu v_r^2$ is the reactant relative translational energy, $\Delta\epsilon_0$ the energy difference between zero-point levels of products and reactants (>0 when endoergic) and ϵ_{int} and ϵ_{int}' the internal energies of reactants and products, respectively; for the probed molecule, $\epsilon_{\text{int}}'(AB) = G(v) + F(J)$. Notice that, in the three atom case, the number of the second (atomic) product internal states, which can be populated by the reaction, is restricted. When excited levels can be reached, conversion factors can be calculated separately for each level, then combined, properly weighted, to obtain the final result. We shall therefore assume in the following a constant internal energy for the

second product. For an outcoming $AB(v,J)$ molecule, the energy available for product translation, ϵ'_{trans}, is thus uniquely determined by (Eq. 7). The product recoil velocity, as defined by (Eq. 6), is also uniquely determined. In four atom reactions, this is no longer the case. The distribution over w', depending upon internal state energy partitioning of the second diatomic product, must be considered.

II.3. Beam density modeling

The next step in the calculation is to model the beam densities. As our primary goal was to analyse our own results from a pulsed beam experiment, we shall model pulsed beam densities. Continuous beams can be treated as a particular case of pulsed beams with infinite pulse duration.

The simplest realistic shape, defined and continuous in all space, is a gaussian function. Both radial and longitudinal gaussian profiles will therefore be considered. Let r_i and q_i be the radial and longitudinal coordinates, respectively. The density is expressed as:

$$n_i = n_i^\circ \exp\{-a_i r_i^2\} \exp\{-b_i(q_i - v_i t)^2\} \tag{8}$$

where n_i° is the maximum density, $a_i = 4 \ln 2/d_i^2$, if d_i is the beam diameter full-width at half-maximum (FWHM), $b_i = 4 \ln 2/(v_i \Delta t_i)^2$, Δt_i is the pulse duration FWHM, and $(q_i - v_i t)$ the distance to the maximum.

In the following, we neglect beam divergence and velocity spread (see above). Each beam is then completely described with only two parameters, a_i and b_i.

Let the origin, O, lie at the crossing point. If one assumes the beam density to be maximum at O and at the probing time, $t = 0$, (Eq. 8) can be written as follows:

$$\begin{aligned} [BC] &= n_1 = n_1^\circ \exp\{-a_1(x^2 + z^2)\} \exp\{-b_1(v_1 t - y)^2\} \\ [A] &= n_2 = n_2^\circ \exp\{-a_2(y^2 + z^2)\} \exp\{-b_2(v_2 t - x)^2\} \end{aligned} \tag{9}$$

II.4. Integration

We can now re-write integral (4), using (Eqs 1, 2 and 9):

$$I(v,J) = B\sigma_R v_r P(v,J) n_1^\circ n_2^\circ \int_{\mathbf{v}_{\text{lab}}} dP^{v,J}(\mathbf{v}_{\text{lab}}) I \tag{10}$$

where:

$$I = (n_1^\circ n_2^\circ)^{-1} \int_{-t_0}^{0} dt \int_{\text{space}} d\tau \, n_1 n_2 \tag{11}$$

and $-t_0$ is a time integration limit discussed later. The integral over space must be carried out with the detection constraint, which can be expressed as:

$$\begin{aligned} x &= v_x t + \delta x \\ y &= v_y t + \delta y \\ z &= v_z t + \delta z \end{aligned} \tag{12}$$

where δx, δy and δz allow for the contribution of molecules produced within a volume equal to ΔV_0 and centred at point $M(v_x t, v_y t, v_z t)$.

Let us introduce the detection constraint in the density expressions (Eq. 9). Integral (11) becomes:

$$I = \int_{-t_0}^{0} dt \exp\{-Xt^2\} \, I_x' I_y' I_z' \tag{13}$$

where the terms independent of position coordinates, after v_j expansion according to (Eq. 5), have been grouped in X (X expansion is given in Appendix).

The integrals over position coordinates, I_l', can be written:

$$I_l' = \int_{-\Delta l/2}^{+\Delta l/2} dl \exp\{-\alpha_l (\delta l)^2\} \exp\{-\beta_l t (\delta l)\} \tag{14}$$

when assuming, to allow for an easy variable separation, the probed volume to be a right-angle parallelepiped ($\Delta V_0 = \Delta x \, \Delta y \, \Delta z$), and the detection yield to be constant; l stands for x, y or z, and α_l and β_l parameters are defined as follows:

$$\begin{aligned} &\alpha_x = a_1 + b_2 \qquad \alpha_y = a_2 + b_1 \qquad \alpha_z = a_1 + a_2 \\ &\beta_x = 2(\alpha_x v_x - b_2 v_2) \qquad \beta_y = 2(\alpha_y v_y - b_1 v_1) \qquad \beta_z = 2\alpha_z v_z. \end{aligned} \tag{15}$$

Before calculating I in the general case, we shall first consider limiting cases of practical interest:

II.4.1. The probed volume is small compared to the beam crossing volume

In this case, $\Delta l \ll d_i$ (for $l = x$, y or z, and $i = 1$ or 2) and therefore $\alpha_l(\Delta l/2)^2 \ll 1$, so $\exp\{-\alpha_l(\delta l)^2\} \approx 1$ and $\exp\{-\beta_l t(\delta l)\} \approx 1 - \beta_l t(\delta l)$. Integrals 14 can thus be simplified:

$$I_l' = \int_{-\Delta l/2}^{+\Delta l/2} dl - \int_{-\Delta l/2}^{+\Delta l/2} \beta_l t(\delta l)\, dl = \Delta l \tag{16}$$

giving (Eq. 11):

$$I = \Delta V_0 \int_{-t_0}^{0} dt \exp\{-Xt^2\} = \tfrac{1}{2}\Delta V_0(\pi/X)^{1/2} \operatorname{erf}\{X^{1/2}t_0\} \tag{17}$$

The integration limit, t_0, is introduced here to allow for experimental limitations, i.e.: molecules produced at too long a time before probing are pumped off, and therefore can no longer contribute to the signal. Such effects generally occur at a much larger time scale than reactive events, especially for pulsed beam experiments. In this case, $t_0 \gg X^{-1/2} \Rightarrow \operatorname{erf}\{X^{1/2}t_0\} \to 1$, giving:

$$I = \tfrac{1}{2}\Delta V_0(\pi/X)^{1/2} \tag{18}$$

For continuous beams, this assumption no longer holds. Furthermore, $X \to 0$ when $\mathbf{v}_{\text{lab}} \to 0$. In the latter case integral becomes $I = \Delta V_0 t_0$, and a definite t_0 value ensures I to be definite. However, a simple way to take such experimental limitations into account is to model continuous beams as "pulsed" beams of duration $\approx t_0$, taken as the mean time between collisions, which may be evaluated from measurement of attenuation of one beam by the other one.

II.4.2. The probed volume is large compared to the beam crossing volume

In this case, all molecules can be regarded as produced at the origin. The detection constraint is then expressed by:

$$|\mathbf{v}_{\text{lab}}t| \leq |\mathbf{r}_0| \tag{19}$$

where $\mathbf{r}_0 = (\Delta x/2, \Delta y/2, \Delta z/2)$. Considering that, for x and $y \approx 0$, $\exp\{2b_1v_1yt\} \approx \exp\{2b_2v_2xt\} \approx 1$, integral (11) becomes:

$$I = \int_{-t_0}^{0} dt \exp\{-\Omega t^2\}\Delta V^* \tag{20}$$

where $\Omega = b_1{v_1}^2 + b_2{v_2}^2 = 4\ \ln 2(\Delta {t_1}^{-2} + \Delta {t_2}^{-2})$, and ΔV^* is the effective beam crossing volume:

$$\Delta V^* = \iiint_{\text{space}} dx\ dy\ dz \exp\{-\alpha_x x^2 - \alpha_y y^2 - \alpha_z z^2\}$$

$$= \pi^{3/2}\{\alpha_x\alpha_y\alpha_z\}^{-1/2}$$

Integration of (Eq. 20) is straightforward:

$$I = \tfrac{1}{2}(\pi/\Omega)^{1/2} \operatorname{erf}(\Omega^{1/2}t_0)\Delta V^* \tag{22}$$

For long pulses, or continuous beams, i.e. for $\Omega \to 0$, (Eq. 22) reduces to:

$$I = t_0\Delta V^* = \Delta V^* \|\mathbf{r}_0\|/\|\mathbf{v}_{\text{lab}}\| \tag{23}$$

In this case, the LIF intensity of a line is simply proportional to the nascent population of the corresponding level divided by the recoil velocity in the laboratory frame, $\mathbf{v}_{\text{lab}}$. This is the DF transformation proposed by Zare and coworkers.[2]

For short pulses, (i.e. for $\Omega^{1/2}\, t_0 \gg 1 \Rightarrow \operatorname{erf}\{\Omega^{1/2}\, t_0\} \to 1$), I is given by:

$$I = \langle \Delta t \rangle\ \Delta V^* \tag{24}$$

where $\langle \Delta t \rangle = \tfrac{1}{2}(\pi/\Omega)^{1/2}$ stands for the effective beam pulse duration. In that case, the intensity is no longer dependent on recoil velocity, but rather simply proportional to the rovibrational population.

II.4.3. General case

Approximations of former cases no longer hold. Expanding the exponential term, $\exp\{-\beta_l t\delta l\}$, in the usual series, one gets the

integral over space:

$$I'_l = \int_{-\Delta l/2}^{+\Delta l/2} dl \exp\{-\alpha_l(\delta l)^2\} \left\{ \sum_{k=0}^{\infty} (-1)^k/k!\ (\beta_l t \delta l)^k \right\}$$
$$= \sum_{k=0}^{\infty} A_l^{2k}\, t^{2k} \tag{25}$$

In fact, due to parity considerations, only even terms, referred to as A_l^{2k}, do not vanish when integrated. They can be calculated by performing a sequence of k integrations by parts.

Noting that:

$$\prod_{n=1}^{k} \{2(k-n)+1\} = 2^k \pi^{-1/2}\, \Gamma(k+\tfrac{1}{2}),$$

it comes:

$$A_l^{2k} = \frac{\beta_l^{2k}\, \Gamma(k+1/2)}{(2k)!\alpha_l^{(k+1/2)}} \left(\operatorname{erf}\{u_l^{1/2}\} - \sum_{m=1}^{k} \frac{u_l^{(k-m+1/2)}}{\Gamma(k-m+3/2)} \exp\{-u_l\} \right) \tag{26}$$

where u_l stands for:

$$u_x = \alpha_x(\Delta x/2)^2 \qquad u_y = \alpha_y(\Delta y/2)^2 \quad \text{and} \quad u_z = \alpha_z(\Delta z/2)^2 \tag{27}$$

Integral (13) becomes:

$$I = \int_{-t_0}^{0} dt \left(\sum_{k=0}^{\infty} A_x^{2k} t^{2k} \right) \left(\sum_{k=0}^{\infty} A_y^{2k} t^{2k} \right) \left(\sum_{k=0}^{\infty} A_z^{2k} t^{2k} \right) \exp\{-Xt^2\} \tag{28}$$

For large values of u_l, (i.e. when $\Delta V_0 \gg \Delta V^*$), it is much simpler to use approximate expressions derived in §II.4.2.

In the intermediate case ($\Delta V_0 \approx \Delta V^*$, $u_l \approx 1$), the expansions in (Eq. 28) can be restricted. The first term of each series will be generally sufficient:

$$A_l^0 = (\pi/\alpha_l)^{1/2} \operatorname{erf}(u_l^{1/2}) \tag{29}$$

Replacing the sum by A_l^0 in (Eq. 28) and integrating (with $t_0 \rightarrow \infty$) yields:

$$I = \tfrac{1}{2}\Delta V^* \text{ erf } (u_x^{1/2}) \text{ erf } (u_y^{1/2}) \text{ erf } (u_z^{1/2}) \ (\pi/X)^{1/2} \tag{30}$$

For small u_l values, erf $(u_l^{1/2}) \rightarrow 2(u_l/\pi)^{1/2}$; integral (30) becomes:

$$I = \tfrac{1}{2}\Delta V^* \ (\pi/X)^{1/2}\pi^{-3/2} \ (\alpha_x\alpha_y\alpha_z)^{1/2}\Delta V_0 \tag{31}$$

which indeed yields the same expression as found in previous section (II.4.1) if one introduces the definition of ΔV^* (Eq. 21).

II.5. Recoil velocity distribution

The final step of calculation is to integrate over product recoil velocity distribution, $dP^{v,J}(\mathbf{v}_{\text{lab}})$:

$$dP^{v,J}(\mathbf{v}_{\text{lab}}) = \frac{\partial^2 P^{v,J}}{\partial\theta \ \partial\phi} \, d\theta \, d\phi \tag{32}$$

Here the modulus of $\mathbf{w}'$ is assumed to be constant (3 atom case). From symmetry considerations for unaligned reactants, the angular distribution is independent of ϕ angle, yielding:

$$dP^{v,J}(\mathbf{v}_{\text{lab}}) = \frac{1}{2\pi} \frac{\partial P^{v,J}}{\partial\theta} \, d\theta \, d\phi \tag{33}$$

Integration over ϕ can be easily carried out numerically, yielding the differential conversion factor:

$$Y(v,J,\theta) = v_r/2\pi \int_0^{2\pi} I \, d\phi \tag{34}$$

The NPMD conversion factor (from nascent population to measured densities) is finally obtained by further integration over the product recoil angle (in the cm frame) distribution:

$$Y(v,J) = \int_0^{\pi} \frac{\partial P^{v,J}}{\partial\theta} Y(v,J,\theta) \, d\theta \tag{35}$$

The LIF intensity of the line(s) corresponding to AB molecules produced in the (v,J) state (Eq. 10) is simply:

$$I(v,J) = B\sigma_R n_1^\circ n_2^\circ P(v,J) Y(v,J) \tag{36}$$

III. APPLICATION TO THE C + NO → CN + O REACTION

We shall now present some results dealing with the C + NO reaction, studied in a pulsed crossed supersonic molecular beam experiment.

These experiments were described elsewhere.[8,9] Briefly, both beams were produced using pulsed nozzles, carbon atoms being obtained by laser vaporisation of graphite, using argon as a carrier gas. En route to a study of the dynamics of this reaction,[10] LIF spectra of CN product ($B^2\Sigma^+ - X^2\Sigma^+$ transition) were recorded under various conditions. In particular, when introducing collimators on the beams, the fluorescence intensity was dramatically lowered, more than expected from the beam density decrease. This discrepancy was thought to result from some "geometrical" aspects, i.e. when reducing the beam crossing volume one also reduced the number of product molecules detected in the probed volume.

We have thus applied our model to C + NO collisions at 0.06 eV relative translational energy. The corresponding Newton diagram is shown in Figure 2. Pulse durations, measured either by fast ionisation gauge (FIG) or LIF profiles at the crossing point, are 20 μs and 35μs for C and NO beams, respectively. NPMD differential conversion factors, $Y(v = 1, K,\theta)$, calculated in the $\Delta V_0 \ll \Delta V^*$ case, are displayed in Figures 3 and 4 as a function of rotational quantum number, $K = J \pm \frac{1}{2}$, and recoil angle in the cm frame, θ.

These results may be interpreted by considering the Newton diagram (Figure 2). Consider a path along which the product of reactant densities would remain almost maximum: concentration of species produced along this path would be maximum, in the probed volume, provided velocities are not too different, i.e. product and reactants moving "in phase". In case of reactant beams of equal diameters, and equal pulse durations, such a path lies along the resultant $\mathbf{v}_C + \mathbf{v}_{NO}$; if one beam (e.g. the carbon beam) is much shorter than the other one, the "maximum" path will tend to align along the direction of this beam ($\mathbf{v}_C$). This is consistent with results of calculations carried out for equal diameters ($d_1 = d_2 = 50$ mm). For equal beam pulse durations ($\Delta t_1 = \Delta t_2 = 35\,\mu$s), a maximum is found at $\theta = 0$, $K = 70$, i.e. $\mathbf{v}_{lab}$ close to the resultant $\mathbf{v}_C + \mathbf{v}_{NO}$ (see Figure 2), whereas shortening C beam duration down to $\Delta t_2 = 5\,\mu$s results in a maximum at $\theta = 0$, $K = 63$, i.e. $\mathbf{v}_{lab}$ close to $\mathbf{v}_C$.

Actual beam durations are intermediate between these two limiting

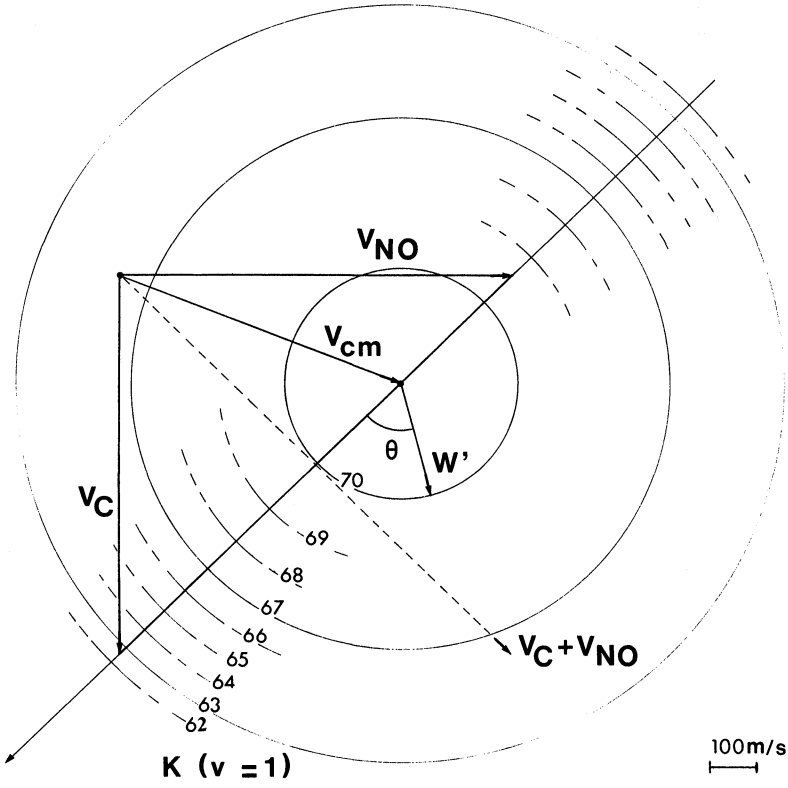

Figure 2 Newton diagram for the C + NO → CN + O reaction in crossed beams at a relative translational energy of 0.06 eV; w′ for CN product in $v = 1$ state.

cases: the carbon beam ($\Delta t_2 = 20\ \mu s$) is somewhat shorter than the NO beam ($\Delta t_1 = 35\ \mu s$). Results obtained for uncollimated beams (cf. Figure 3a) are therewith consistent, yielding a maximum for $\theta = 0$, $K = 67$, i.e. products recoiling forward with a velocity in the laboratory frame intermediate between $\mathbf{v}_C$ and the resultant $\mathbf{v}_C + \mathbf{v}_{NO}$. Calculations for uncollimated beams are possible, since, in our experiments, the crossing point is far enough from the nozzles (80 mm for NO and 110 mm for C), resulting in a divergence of $\approx 30°$ FWHM; the assumption of ideal beams, although crude in this case, remains nonetheless reasonable.

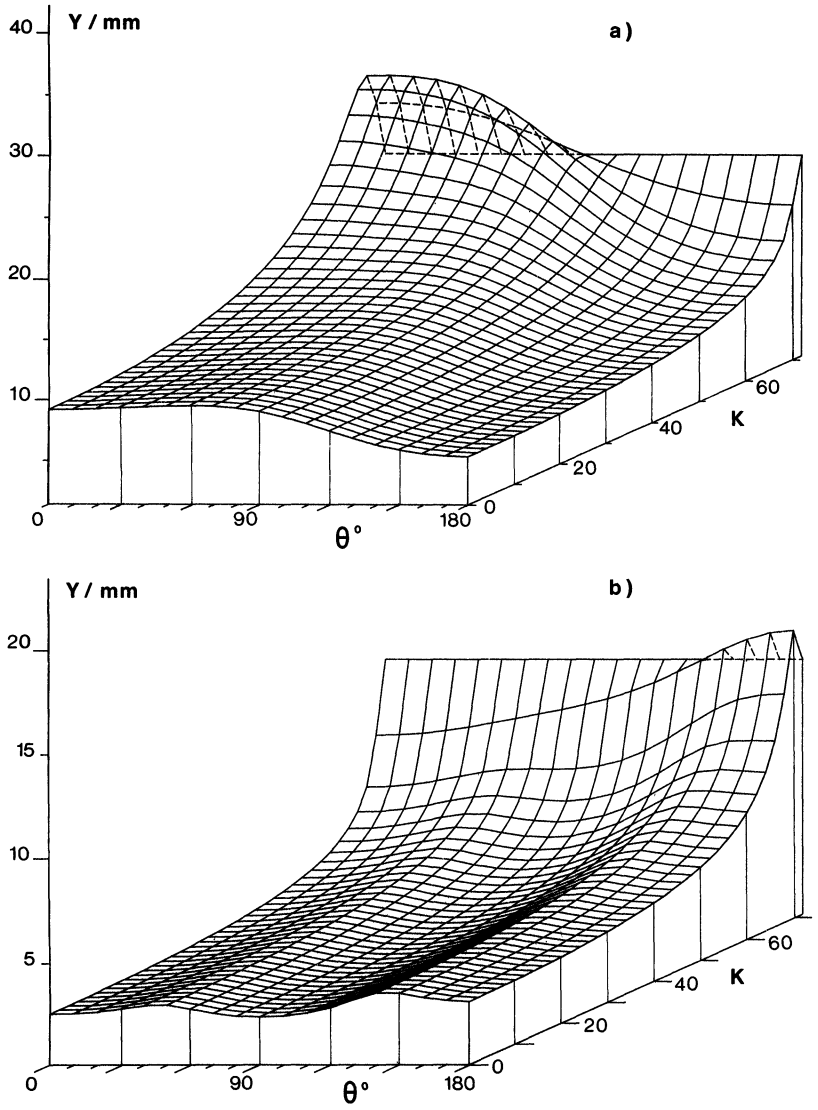

Figure 3 Population to density differential conversion factor, $Y(v = 1, K,\theta)$, as a function of energy available to translation, and recoil velocity orientation in the cm frame, θ; energy is scaled in units of rotational quantum number, K, of the $v = 1$ vibrational level; lines of the axonometric plot are spaced by 10° along θ axis, and by a ΔK interval of 2 along the K axis; a: uncollimated beams; b: collimator (∅ 2 mm) on NO beam.

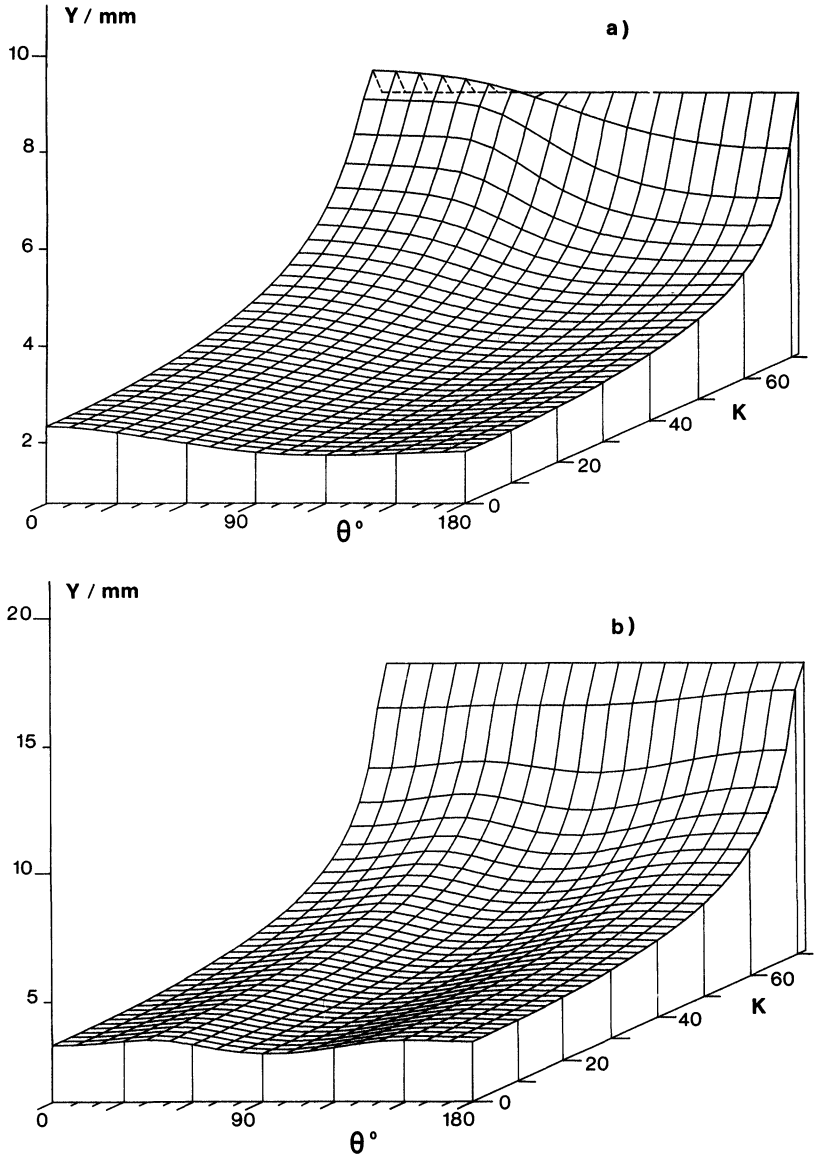

Figure 4 Population to density differential conversion factor, $Y(v = 1, K, \theta)$ (see Figure 3); a: collimators (∅ 2 mm) on both beams; b: collimators of ∅ 5 and ∅ 10 mm on NO and C beams, respectively.

It is worth noting that a maximum in detection efficiency could be expected for molecules produced with a low velocity in the laboratory frame. In the example of Figure 2, this may occur for CN produced in the $v = 1$, $K = 66$ state, and scattered at $\theta \approx 60°$, in the plane of the beams ($\phi = 180°$). As, for a given θ, scattering is equally probable at any ϕ angle, a maximum will not necessarily arise from this particular situation, with the exception of continuous beam experiments, where accumulation of low velocity products in the probed volume may occur (see above).

Effects due to the shorter pulse duration of one beam (here the carbon beam) can be counterbalanced by collimating the "longer" one (NO). Furthermore, under severe collimation conditions (cf. Figure 3b), detection is more efficient for species scattered backward, rather than forward, with a maximum close to excitation limit ($K = 69$), $\mathbf{v}_{lab}$ lying almost along $\mathbf{v}_{NO}$: enhancement then occurs along that direction since the carbon beam is much larger than the NO beam.

When the beams are equally collimated (cf Figure 4a), the situation is similar to the uncollimated case, apart from the dramatic decrease in detection efficiency.

The last case explored (Figure 4b), with ∅5 mm and ∅10 mm collimators on the NO and C beams, respectively, shows that both effects (i.e. shorter C pulse duration and narrower NO beam) can be balanced, resulting in a detection efficiency almost independent of the recoil direction.

Following theoretical calculations[11] in favour of a "rebound" type mechanism, the angular distribution has been assumed to be mainly "backward" ($\theta = \pi$), and simply modelled by a $\sin^2(\theta/2)$ function. Conversion factors, $Y(v,J)$, are obtained by integration over this distribution (Figure 5). Relative intensities of CN(B–X) (0–1) band-head can then be determined from reactant beam densities under various conditions (Table 2). The results are in good agreement with experimental values.

CONCLUSION

The model provides a convenient way to take into account experimental conditions when relating nascent populations to LIF intensities. It points out the dependence of LIF detection on experimental factors, such as pulse durations (for pulsed beams) and beam collimation. The

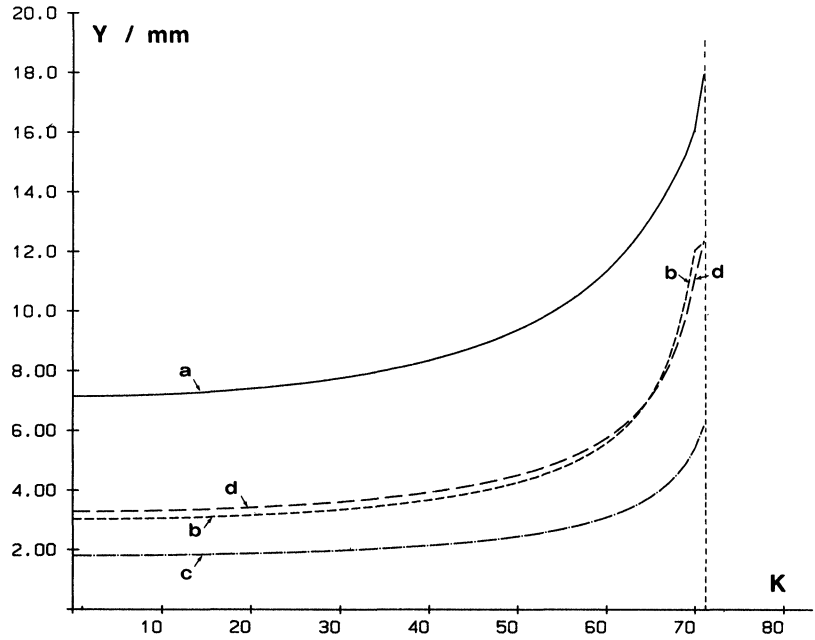

Figure 5 Conversion factors integrated over a "backward" angular distribution; a: uncollimated beams; b: collimator (Ø 2 mm) on NO beam; c: collimators (Ø 2 mm) on both beams; d: collimators of Ø 5 and Ø 10 mm on NO and C beams, respectively.

Table II C + NO → CN + O reaction.

NO beam[a]		C beam[a]							
ϕ_{col}	d_1	ϕ_{col}	d_2	$I(NO)$[b]	$I(C)$[c]	$I(NO)I(C)$	Y_H[d]	$I_c(CN)$[e]	$I(CN)$[f]
n[g]	≥50	n	≥50	———			1	———	
5	7.5	10	20	0.75	0.68	0.51	0.46	0.23_5	0.25
2	5.6	n	≥50	0.27	1	0.27	0.43	0.12	0.133
2	5.6	2	6	0.27	0.31	0.084	0.255	0.021	≤0.033

Notes and symbols: a) all dimensions are in mm; beam profiles are determined using a fast ionisation gauge (FIG) displaced across the beams; b) relative NO density is estimated from FIG measurements; c) relative C density is derived from LIF measurements of C_2 (Swan system): as source conditions do not vary, the C/C_2 ratio is assumed to remain constant whatever collimator is used; d) Y_H stands for the conversion factor, relative to the uncollimated case value, calculated at the 0–1 bandhead; e) $I_c(CN) = I(NO)\ I(C)\ Y_H$; f) experiment; g) n: no collimator.

latter factor, in particular, has been shown to be of crucial importance, especially when collimators of different diameters are used, which may result in a high anisotropy in detection efficiency with respect to product recoil direction.

References

1. J. L. Kinsey, *Ann. Rev. Phys. Chem.* **28,** 349 (1977).
2. H. W. Cruse, P. J. Dagdigian and R. N. Zare, *Faraday Disc. Chem. Soc.* **55,** 277 (1973).
3. U. Fano and J. H. Macek, *Rev. Mod. Phys.* **45,** 553 (1973).
4. C. H. Greene and R. N. Zare, *J. Chem. Phys.* **78,** 6471 (1983).
5. R. Altkorn and R. N. Zare, *Ann. Rev. Phys. Chem.* **35,** 265 (1984).
6. N. Billy, B. Girard, G. Gouédard and J. Vigué, *Mol. Phys.* **61,** 65 (1987).
7. B. Girard, Thèse d'Etat, Université Pierre et Marie Curie (Paris VI), Paris, 1987.
8. G. Dorthe, M. Costes, C. Naulin, C. Vaucamps, G. Nouchi and J. Joussot-Dubien, *C. R. Acad. Sc. Paris,* **II 301,** 9 (1985).
9. G. Dorthe, M. Costes, C. Naulin, J. Joussot-Dubien, C. Vaucamps and G. Nouchi, *J. Chem. Phys.* **83,** 3171 (1985).
10. M. Costes, G. Dorthe, B. Duguay, P. Halvick, J. Joussot-Dubien, C. Naulin, G. Nouchi, J. C. Rayez, M. T. Rayez and C. Vaucamps, *Recent Advances in Molecular Reaction Dynamics,* R. Vetter and J. Vigue (eds.), Editions du C.N.R.S., Paris, 1986, p. 97.
11. P. Halvick, Thèse d'Etat, Université de Bordeaux I, Talence, 1987.

APPENDIX

The X term introduced in (Eq. 13) is defined as follows:

$$X = A_0 + A_X w'_X/v_r + A_Y w'_Y/v_r + A_{XY} w'_X w'_Y/v_r^2 \ldots + A_X^2 (w'_X/v_r)^2 + A_Y^2 (w'_Y/v_r)^2 + A_Z^2 (w'_Z/v_r)^2 \quad \text{(A1)}$$

where:

$$\begin{aligned} A_0 &= v_1^2(a_2\lambda_2^2 + b_1\lambda_1^2) + v_2^2(a_1\lambda_1^2 + b_2\lambda_2^2) \\ A_X &= 2v_1^2(b_1\lambda_1 - a_2\lambda_2) + 2v_2^2(a_1\lambda_1 - b_2\lambda_2) \\ A_Y &= 2v_1v_2\{(a_1 - b_1)\lambda_1 + (a_2 - b_2)\lambda_2\} \\ A_{XY} &= 2v_1v_2(a_1 - b_1 - a_2 + b_2) \\ A_X^2 &= v_1^2(a_2 + b_1) + v_2^2(a_1 + b_2) \\ A_Y^2 &= v_1^2(a_1 + b_2) + v_2^2(a_2 + b_1) \\ A_Z^2 &= v_r^2(a_1 + a_2) \end{aligned} \quad \text{(A2)}$$

A more useful form for calculation can be obtained for X by introducing the w'_j expressions given in Table I. Let $s = w'/v_r$; it comes:

$$X = A_0 + A_X s \cos\theta + A_Y s \sin\theta + A_{XY} s^2 \sin\theta \cos\theta \cos\phi \ldots + A_X{}^2 s^2 \cos^2\theta + A_Y{}^2 s^2 \sin^2\theta \cos^2\phi + A_Z{}^2 s^2 \sin^2\theta \sin^2\phi \quad \text{(A3)}$$